npj | materials degradation

Article

Published in partnership with CSCP and USTB

https://doi.org/10.1038/s41529-024-00445-x

Mechanisms and energetics of calcium aluminosilicate glass dissolution through ab initio molecular dynamics-metadynamics simulations

Meili Liu & Luis Ruiz Pestana

The dissolution of silicate glasses has implications in diverse fields ranging from the immobilization of radioactive waste to the development of sustainable alternatives to Portland cement. Here, we used ab initio molecular dynamics simulations biased with well-tempered metadynamics to study Si-O-T bridge dissociation in calcium aluminosilicate glasses, crucial for understanding their dissolution. In a departure from the conventional Michalske-Freiman model, our findings reveal a nucleophilic substitution reaction mechanism characterized by a short-lived, 5-fold coordinated Si intermediate or transition state, depending on the Si bridge coordination, with a near-trigonal bipyramidal geometry. We find that the reorganization required for reaching this state causes the activation energy barriers to be dependent on the Si bridge coordination, with Si Q^3 species serving as the rate-limiting step in the dissolution reaction. Our findings not only challenge long-standing theoretical models but also pave the way for more accurate and comprehensive frameworks for understanding the dissolution of silicate glasses in various applications.

The aqueous corrosion of silicate glasses plays a key role in a broad range of applications, from the immobilization of radioactive waste to biomedical uses[1,2]. Understanding the dissolution of calcium aluminosilicate (CAS) glasses, in particular, is critical to the development of sustainable alternatives to Portland cement[3], a primary contributor to the environmental impact of concrete—the most widely used material worldwide. At short- and medium-range length scales, CAS glasses consist of a disordered network of silicon (Si) and aluminum (Al) atoms connected by oxygen (O) atoms through T-O-T' bridges, where T and T' can be either Si or Al. The calcium (Ca^{2+}) ions in the glass disrupt these bridges, effectively depolymerizing the network. Within the glasses, Si atoms exist in different polymerization states, which we refer to as Si Q^n, where n = 1, 2, 3, or 4 indicates the number of Si-O-T bridges associated with the Si atom. Kinetic Monte Carlo (KMC) methods have shown significant promise for simulating the dissolution process of silicate glasses on time scales commensurate with experimental measurements[4–8]. However, for these methods to be successful, a precise quantitative understanding of the energetics and mechanisms at the molecular level, where dissolution of silicate glasses proceeds through the sequential hydrolysis of Si-O-T bridges, is critical.

Since the early work of Lasaga[9], electronic structure methods have become indispensable tools for studying Si-O-Si bridge dissociation. Pelmenschikov et al.[10] calculated, using density functional theory (DFT) simulations of small clusters of β-cristobalite and a single water molecule, a Si-O-Si bridge dissociation activation energy for Si Q^2 species of 29 kcal·mol^{-1}. Based on the discrepancy between the calculated value and the experimentally measured activation energies[11,12], they proposed it must be the dissociation of the last Si-O-Si bridge (i.e., Si Q^1) that governs the dissolution kinetics of silica. Later, Criscenti et al.[13] used DFT calculations of a small cluster representative of Si Q^3 interacting with a handful of water molecules to investigate the Si-O-Si dissociation reaction catalyzed by hydronium ions (H_3O^+). Based on their calculated activation barrier of 26.75 kcal mol^{-1}, they concluded that the dissociation of bridges associated to Si Q^2 must be the rate-limiting step during dissolution.

Much of the existing literature has focused on the dissociation of Si-O-Si bridges associated with two-membered (2M) silicon rings, sometimes referred to as ring defects[14–18]. Rimsza and Du[17], through unbiased ab initio molecular dynamics (AIMD) simulations of nanoporous silica, observed a 5-fold coordinated Si intermediate state during the removal of 2M ring defects. This observation is consistent

Civil and Architectural Engineering, University of Miami, Coral Gables, FL, USA. e-mail: luisruizpestana@miami.edu

with the classical Michalske-Freiman mechanism proposed in 1983[19], which has been commonly accepted by the community. Namely, a water molecule adsorbs in the vicinity of the bridge, followed by an intermediate state where the water oxygen coordinates to the Si, which becomes pentacoordinated, while one of the hydrogens of the water molecule forms a hydrogen bond with the bridging oxygen. Finally, that proton transfers to the bridging oxygen and the Si-O bond dissociates, creating two silanol groups (Si-OH). Masini and Bernasconi[14] used Car-Parrinello molecular dynamics (CPMD) simulations and the method of constraints[20] to calculate an activation barrier of 7.4 kcal·mol^{-1} for the dissociation of the Si-O bond in 2M rings through a mechanism where the bridging oxygen bonds to the nucleophile's hydrogen. Interestingly, they found a much higher energy barrier (25.4 kcal mol^{-1}) when the reaction proceeded through a different pathway involving a 5-fold coordinated Si intermediate. Nonetheless, the representativeness of their findings is potentially limited by their highly simplified water interface model, which included only one water molecule. While, as shown by Ceresoli and co-workers[21], 2M ring defects are expected on dry silica surfaces, they are virtually absent in bulk glasses[22], and are also not expected to be significant on hydrated surfaces, such as those of interest in our study. Furthermore, while these defects are considered to be the most reactive sites on the surface, and thus of interest for certain applications, they are not likely to be the rate-limiting step controlling the dissolution kinetics of CAS glasses.

Very few studies have ventured beyond pure silicate systems. Wallace et al.[23] showed that cations in solution, such as Ca^{2+}, reduce the activation barrier for Si-O-Si dissociation when coordinated to the silicate as inner-sphere complexes. Garrison and co-workers showed[24], using DFT simulations of small aluminosilicate clusters, that the activation energy for the dissociation of T-O-T' bridges associated to either Si or Al Q^1 depends not only on the type of bridge (Si-O-Si or Si-O-Al), but also on the protonation state of the terminal sites. Recently, Izadifar et al.[25] used DFT simulations of small aluminosilicate clusters and a single water molecule as a hydrolyzing agent to investigate the differences in activation barriers between Si-O-Si and Si-O-Al bridges. However, the differences in degree of polymerization and oxygen coordination between the Si and Al species involved were not considered.

Whether the Michalske-Freiman model accurately captures Si-O-T bridge dissociation in CAS glasses, and how the energetics of Si-O-T dissociation are influenced by the coordination of the Si species, remain unanswered questions. This uncertainty partially arises because previous studies based on electronic structure methods have often relied on over-simplified, small model systems that either inadequately represent the complexity and condensed matter character of the glass surface or the behavior and dynamics of liquid water at the interface with the glass. It is also worth noting that differences in methodological details can affect greatly both the mechanisms and energetics of the reactions as illustrated in Table 2 in Ref. [13] or Table 3 in Ref. [18]. Distinguishing between methodological effects and inherent physical phenomena can be challenging.

MD simulations based on reactive force fields have also been employed to study the molecular mechanisms and energetics of silica dissolution[18,26,27]. For example, Garofalini and co-workers[26] found that the activation energy barrier for bridge dissociation decreases with the polymerization degree of the Si species. Intriguingly, they identified an S_N2-type reaction mechanism that diverges significantly from the Michalske-Freiman model in that the bridge opposite and colinear to the newly coordinated nucleophile is the one that dissociates. The activation barriers they reported were significantly lower compared to those obtained using ab initio methods, and the variation in activation barriers between different Si species was found to be very modest—factors which may emerge from the limited accuracy of the force field used to describe the potential energy surface. Simulations using a reparametrized reactive force field (ReaxFF) have also been reported recently[18,27]; however, these studies primarily focused on the formation of silanol groups on the hydrated silica surface, rather than the dissociation of T-O-T' bridges. Recently, Du and co-workers employed reactive molecular dynamics simulations to study sodium aluminosilicate glasses, shedding light on the role that aluminum plays on rapid surface reactions of these glasses with water. While the precise free energies were not quantified, the unbiased simulations revealed that bridges involving aluminum underwent more transformations during the simulations than those including silicon, suggesting the greater stability of the latter[28,29].

Overall, simulations that simultaneously account for the structural and compositional complexity of CAS glasses, the behavior of liquid water at the interface, use minimally biased free energy methods, accurately represent the potential energy surface, and that cover Si species with different bridge coordination environments in the glasses are lacking. In this study, we aim to address these challenges by using ab initio molecular dynamics (AIMD) simulations based on Density Functional Theory (DFT) and biased with well-tempered metadynamics (WTMetaD). Our goal is to elucidate the reaction mechanism and free energy of the hydrolysis of Si-O-T bridges associated to Si Q^1, Q^2, and Q^3 species in a realistic CAS glass surface in contact with liquid water at ambient temperature.

Results

In the first subsection, we discuss the mechanisms and energetics of the Si-O-T dissociation reaction analyzed from three converged AIMD-WTMetaD simulations involving Si Q^3, Q^2 and Q^1 species on a CAS glass surface in equilibrium with liquid water (Fig. 1). In the subsections after that, we draw on short AIMD-WTMetaD runs, terminated following the bridge dissociation event, which we used to validate the robustness of the nucleophilic substitution mechanism observed in our three well-converged simulations. We carried out 10 independent AIMD-WTMetaD runs for each of 6 different Si atoms on the CAS glass surface. Snapshots of the specific Si atoms and their local CAS glass environment are shown in Supplementary Figure 1.

Energetics and mechanism of Si-O-T dissociation

We perform AIMD-WTMetaD simulations to study the energetics and reaction mechanisms driving the dissociation of Si-O-T bridges in a CAS

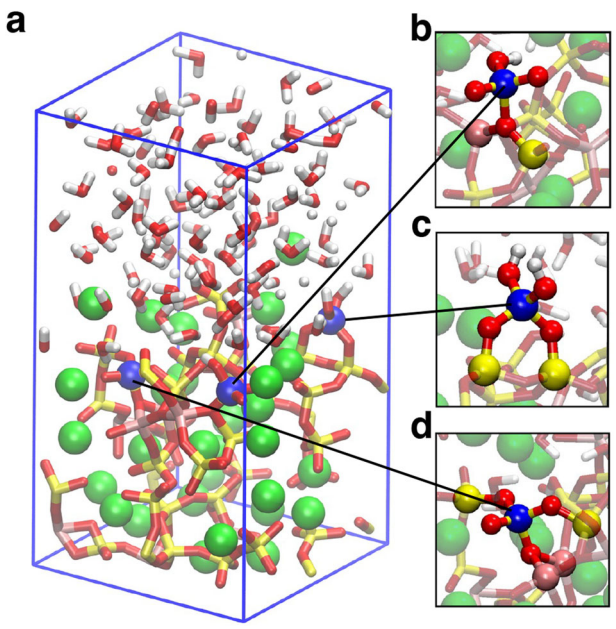

Fig. 1 | Atomistic representation of the hydrated CAS glass system and the Si species analyzed in the converged AIMD-WTMetaD simulations. a Snapshot of the simulated CAS glass in equilibrium with liquid water. Elements are color-coded as follows: calcium (green), hydrogen (white), oxygen (red), silicon (yellow), and aluminum (pink). **b**–**d** Snapshots of the Si Q^1, Q^2, and Q^3 species (shown in blue), respectively, analyzed in the converged AIMD-WTMetaD simulations.

glass surface that is in equilibrium with liquid water (Fig. 1a). Specifically, we map the free energy surface (FES) of the bridge dissociation reaction for the Si Q^1, Q^2, and Q^3 species shown in Fig. 1b–d, respectively.

Figure 2 displays the FES obtained from the AIMD-WTMetaD simulations as well as the free energy profiles along the minimum energy path (MEP) of the reactions. The MEPs are calculated using the finite temperature string method[30], following a protocol outlined in one of our previous publications[31]. The FES are converged to within 2 kcal mol^{-1} after observing multiple recrossing between reactants and products during the simulations (Supplementary Figure 2). It is important to note that our simulations provide quantitative insights into the free energy of the reactants, transition, and intermediate states, but not the product state. The free energy of the products is biased due to the use of wall potentials in our simulations near the product state (shown as red dashed lines in Fig. 2a, c, e). We implemented these walls to facilitate recrossing between reactants and products, enhancing the sampling of the transition state and thereby facilitating the convergence of the free energy surface and ensuring a more reliable estimate of the activation free energy barrier.

The choice of collective variables (CVs) plays a pivotal role for accurately distinguishing the reactants, products, and transition state of the Si-O-T bridge dissociation reaction. For systems involving Si Q^3 and Q^2 species, we defined two distinct CVs based on the oxygen coordination to the Si atom. The first CV, denoted as CN(Si-O_b) and represented on the y-axis of the free energy plots in Fig. 2, measures the coordination number of bridging oxygens (O_b) to the Si atom. This coordination number is calculated using a continuous and differentiable switching function, as shown in Eq. 1 in the Computational Methods section. The second CV, CN(Si-O_W), displayed on the x-axis of the free energy plots in Fig. 2, quantifies the coordination number of non-bridging or hydroxyl oxygens (O_w) to the Si atom. For the Si Q^1 system, where only one bridging oxygen is present, the CV associated to O_b coordination becomes redundant. Hence, in this case, we replaced it with a new CV, Dist(Si-O_b), which measures the distance between the Si atom and the oxygen of the bridge that is undergoing dissociation. We opted not to study Si Q^4 species here because previous work[26] suggests they are neither particularly abundant on the glass surface nor play a rate-limiting role in the dissolution process.

From the examination of the FES presented in Fig. 2a, c, e, and after careful analysis of the simulation trajectories, we have deduced the following mechanistic behavior. Initially, a nucleophile, typically a water molecule, approaches the Si atom, often after forming a hydrogen bond with adjacent silanol groups or non-bridging oxygens (NBOs). The formation of a pentacoordinated Si atom with a near-trigonal bipyramidal shape configuration follows, which we refer to as Si^5 from now on. The stability of this Si^5 state depends on the bridge coordination of the Si. For Si Q^1, it is a transition state; for Si Q^2, it becomes a neutrally metastable intermediate; and for Si Q^3, a shallow metastable intermediate state. These variations are clear in the MEPs shown in Fig. 2b, d, f. Following the Si^5 state, the nucleophile donates a proton to either a water molecule in the liquid (forming a hydronium ion) or to a nearby NBO, but importantly never to a bridging (BO) oxygen. As we will discuss later in more detail, this proton transfer step can also occur at other stages during the reaction. The final step involves the dissociation of the Si-O bond directly opposite and co-linear to the coordinated nucleophile. In Si Q^1 (Fig. 2a, b), nucleophile coordination and Si-O bond dissociation occur simultaneously, while for Si Q^2 and Q^3 species the L-shape of the MEP on the FES suggests a step-wise mechanism.

The described reaction mechanism that we observe for all Si species diverges significantly from the commonly assumed mechanism for siloxane bridge dissociation, as proposed by Michalske and Freiman[23] (Fig. 2g). Instead, as shown in Fig. 2h, the mechanism reported here closely resembles a nucleophilic substitution reaction, which is pervasive in various organic chemistry applications, such as the methylation of halide ions and alcohol dehydrohalogenation. The role of nucleophilic substitution reactions in the polymerization and depolymerization of silicate melts has only recently begun to be recognized[32]. Our study confirms the findings by Kagan et al.[26] that bridge dissociation in silicate glasses occurs through a nucleophilic substitution reaction, but also uncovers previously unseen complexities, including the fact that the nature of the Si^5 state and the activation free energy, as discussed below, depend on the Si bridge coordination .

In regard to the energetics of the Si-O-T dissociation reaction, we observe the activation free energy decreases with the number of bridges initially associated to the Si atom: 19.3 kcal mol^{-1} for Si Q^3, 16.9 kcal mol^{-1} for Si Q^2, and 13.0 kcal mol^{-1} for Si Q^1. While a direct comparison with experiments is not straightforward as reported activation barriers are for pure silica polymorphs, whereas our study specifically investigates Si Q^n in CAS glasses, our results align well within the range of experimental data reported in literature[11,12]. For an in-depth comparison, Supplementary Table 1 offers a comprehensive overview of the activation energy barriers for Si-O-T bridge dissociation, encompassing data from both experiments and prior computational studies on related systems. The observed trend of a diminishing activation free energy as Si bridge coordination decreases can be, at least, partially explained based on the energy necessary to reorganize the local structural environment of Si to accommodate the Si^5 intermediate (or transition) state—from a tetrahedral configuration to a near-trigonal bipyramidal geometry. Such reorganization becomes increasingly cumbersome as the number bridges associated to the Si increases, thereby leading to an increase in the activation energy. It is worth noting that the change in activation energy with the number of bridges is not uniform. We observe a larger decrease when going from Si Q^2 to Si Q^1 than from Si Q^3 to Si Q^2. A second contributing factor to the lower activation barrier is the enhanced ability of lower-coordinated Si species to attract nucleophilic water molecules, owing to their increased number of silanol groups. Further research is however required to characterize the quantitative impact of each of these two mechanisms on the activation barriers.

Our results suggest that the rate limiting step in the dissolution of Si in CAS glasses, which proceeds through the sequential dissociation of Si-O-T bridges, is the transition from Si Q^3 to Si Q^2, which is in qualitative agreement with one previous MD study[24] but not with previous ab initio works where Si Q^2, or even Si Q^1 have been proposed as limiting steps[10,13]. Our results support the notion that the oversimplified nature of the cluster systems typically used in ab initio studies, combined with a lack of conformational sampling at finite temperatures and absent real hydration dynamics, have yielded observations that likely depart from those observed in real-world systems.

Nucleophile approach and coordination to Si

The first step during the Si-O-T dissociation reaction is the approach of the nucleophile to the Si. Due to their polar nature and the ability to form hydrogen bonds, water molecules are particularly attracted to silanol groups and NBOs present on the surface of the glasses. Water molecules and silanol groups can act as both hydrogen bond donors and hydrogen bond acceptors, and NBOs have lone pairs of electrons that can act as hydrogen bond acceptors. We observed that in about 76% of the 60 short AIMD-WTMetaD simulations, the nucleophile was a water molecule that had previously formed a hydrogen bond with either a silanol group or NBO. This observation doesn't serve as proof, but it aligns with the hypothesis that Si atoms with lower bridge coordination tend to exhibit lower activation energies thanks to their enhanced ability to attract nucleophiles. It is worth noting that the water molecule that ended up acting as the nucleophile fluctuated even among independent runs of the same Si atom, which contributes to the robustness of the statistics.

In approximately 15% of the simulations, a nearby silanol group coordinated to a neighboring Si atom acted as the nucleophile in the bridge dissociation reaction. In such cases, the reaction proceeded as follows. First, the proton of the silanol group gets transferred to a water molecule in the liquid (Fig. 3a). Then, then dangling reactive oxygen forms a bond with the Si (Fig. 3b), establishing the Si^5 intermediate state. Finally, the Si-O opposite and co-linear to the nucleophile breaks (Fig. 3c). Of the few simulations involving a silanol group as nucleophile, 45% involved the Si Q^1 (shown in Supplementary Figure 1d), and the remaining 55% involved the Si Q^2 as shown in Fig. 3 and Supplementary

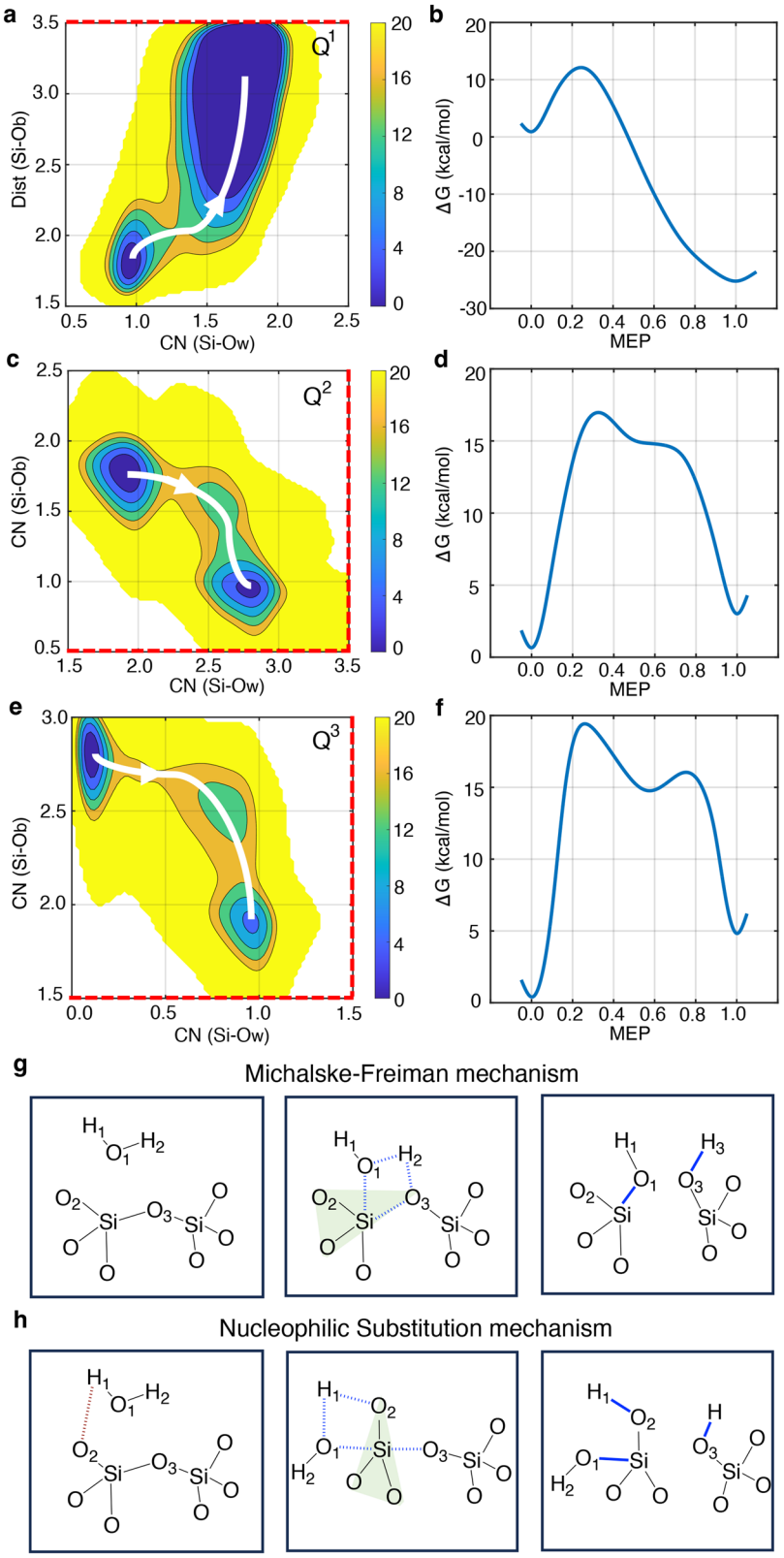

Fig. 2 | Free Energy Surfaces and Reaction Mechanisms of Si-O-T dissociation. a, **c**, **e** display the free energy surfaces reconstructed from the AIMD-WTMetaD simulations for Si Q^1, Q^2, and Q^3, respectively. In those plots, CN(Si-O_b) is the number of bridge oxygens coordinated to the Si atom, CN(Si-O_W) is the number of oxygens in silanol groups coordinated to the Si atom, and Dist(Si-O_b) is the bond length of the dissociated Si-O bond. The MEPs are shown on the FES as white lines. The wall potentials used in the simulations are shown as red dashed lines. **b**, **d**, **f** show the free energy along the MEPs for Si Q^1, Q^2, and Q^3, respectively. The reaction coordinate is 0 at the minimum energy point of the basin corresponding to the reactants, and 1 at the minimum energy point of the basin corresponding to the products. **g** Illustration of the Michalske-Freiman mechanism, typically assumed for the Si-O-T dissociation reaction. **h** Illustration of the nucleophilic substitution reaction mechanism observed in this study.

Figure 1a. In all those instances, although an Si-O-T bridge dissociation event occurs, it ultimately leads to the formation of a two-membered (2 M) silica ring, as illustrated in Fig. 3c. It should be noted that although the formation of 2 M ring defects is observed in some of our simulations, they are not anticipated to be long-lasting in extended, unbiased simulation scenarios.

Pentacoordinated Si intermediate/transition state and Si-O dissociation

As illustrated in Fig. 2, the dissociation of Si-O-T bridges features a Si^5 state characterized by a near-trigonal bipyramidal geometry (Fig. 4a), where the oxygen of the nucleophile, O_w, and the bridging oxygen that is about to dissociate, O_b, occupy the axial positions, as evidenced by

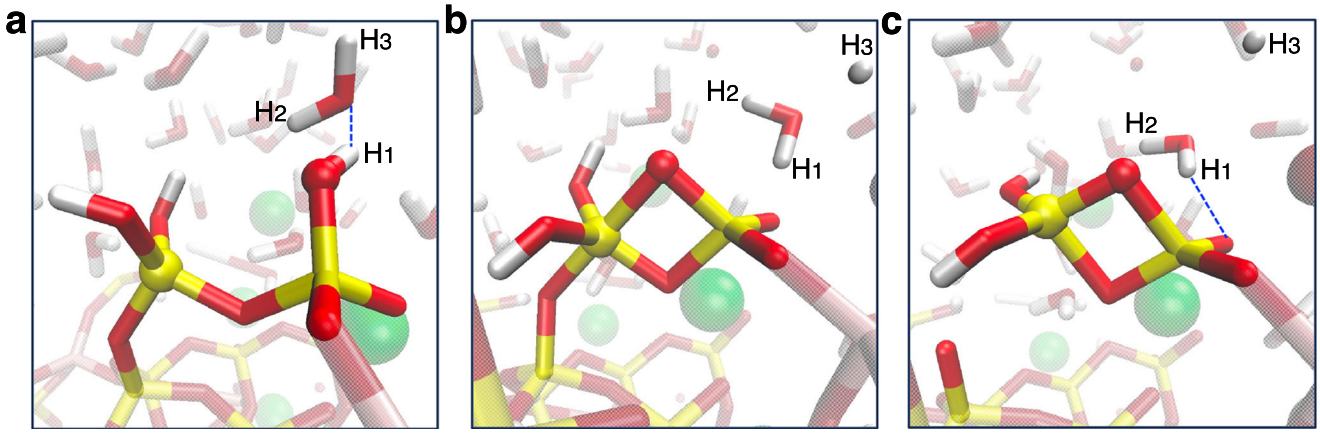

Fig. 3 | Snapshots illustrating the key steps in Si-O-T dissociation with a silanol group acting as nucleophile. a Initial stage showing a hydrogen-bond interaction between the silanol group that will act as nucleophile and a water molecule. **b** The proton from the silanol group transfers to the hydrogen bonded water molecule, which subsequently, following a Grotthuss mechanism, transfers to another water molecule in the liquid. The remaining reactive oxygen forms a new bridge with the Si atom, which adopts a 5-fold coordinated intermediate state. **c** The Si-O bond opposite to the newly formed bridge undergoes dissociation.

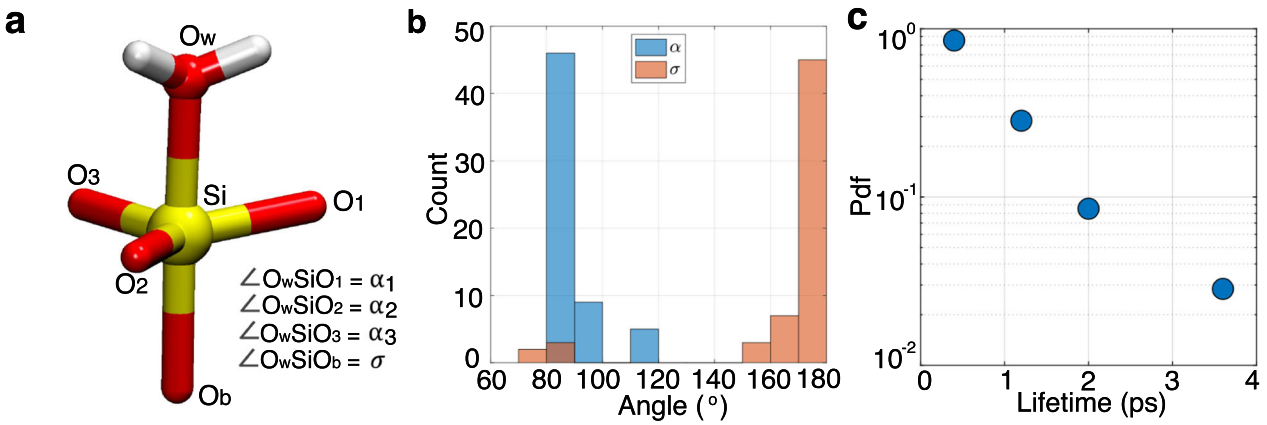

Fig. 4 | Characteristics of the Si^5 state in the Si-O-T dissociation process. a A snapshot illustrating the geometric configuration of the Si^5 state. **b** Histogram showing the distribution of angles $\bar{\alpha}$ and σ, as defined in **a**, aggregated from all simulations. **c** Probability distribution of the lifetime of the Si^5 intermediate state across simulations.

the distribution of angles $\bar{\alpha}$ and σ measured from the simulations (Fig. 4b). As mentioned earlier, the Si^5 state is a transition state for Si Q^1, a neutrally metastable intermediate for Si Q^2, and a shallow metastable intermediate state for Si Q^3. Figure 4c shows the distribution of the lifetime of the Si^5 state from all 60 short AIMD-WTMetaD simulations, which displays an exponential distribution. The average lifetime of the Si^5 state measured from the simulations increases with bridge coordination: 0.56 ps for Q^1, 0.69 ps for Q^2, and 0.89 ps for Q^3. Only in about 8% of the simulations, the Si-O bond that dissociated was not co-linear and opposite to the nucleophile, and these instances only happened for the Si Q^1 cases. These latter cases correspond to the small peak around 80° of the distribution of $\bar{\alpha}$ in Fig. 4b.

Proton transfer from the nucleophile

In the final step leading up to the dissociation of the Si-O bond, a proton transfers from the coordinated nucleophile to become a silanol group (i.e., from Si-H_2O to Si-OH). The proton can transfer to a water molecule in the liquid or to a BO or NBO in the glass. We observe that, if a Si species is coordinated to an NBO that is already hydrogen-bonded to another water molecule from the liquid, or if there is no NBO, the proton from the coordinated nucleophile is typically transferred to other water molecules in the liquid (Fig. 5a). In contrast, if an NBO is present, but it is not hydrogen-bonded to another water molecule, the proton from the water nucleophile invariably transfers to that NBO (Fig. 5b). We only observed a single instance where the proton from the coordinated nucleophile transferred to a bridging (BO) oxygen (Fig. 5c), as posited by the Michalske-Freiman model, and assumed in most earlier ab initio studies. This leads us to conclude that transferring a proton to the BO is not a necessary condition for Si-O bond dissociation. Instead, we expect the real mechanism of Si-O-T dissociation to align closely with a nucleophilic substitution model. The timing at which the proton transfer from the nucleophile takes place varies among the simulations. In approximately 46% of the simulations, the proton transfer occurs concurrently with the Si-O bond dissociation. In about 29% of cases, it happens after the Si-O bond has already broken. In such instances, the proton is consistently transferred to a water molecule. In the remaining 25% of simulations, the proton transfers before the Si-O bond dissociates. In these cases, the proton transfers to liquid water in about half of the occurrences, and to a NBO in the other half.

Discussion

Here, we have investigated the energetics and mechanisms of Si-O-T bridge dissociation in a realistic, hydrated CAS glass environment using ab initio Molecular Dynamics (AIMD) simulations enhanced with Well-Tempered Metadynamics (WTMetaD). We have identified a mechanism for Si-O-T bridge dissociation that diverges from the classical Michalske-Freiman model, which has long informed our understanding of silicate dissolution.

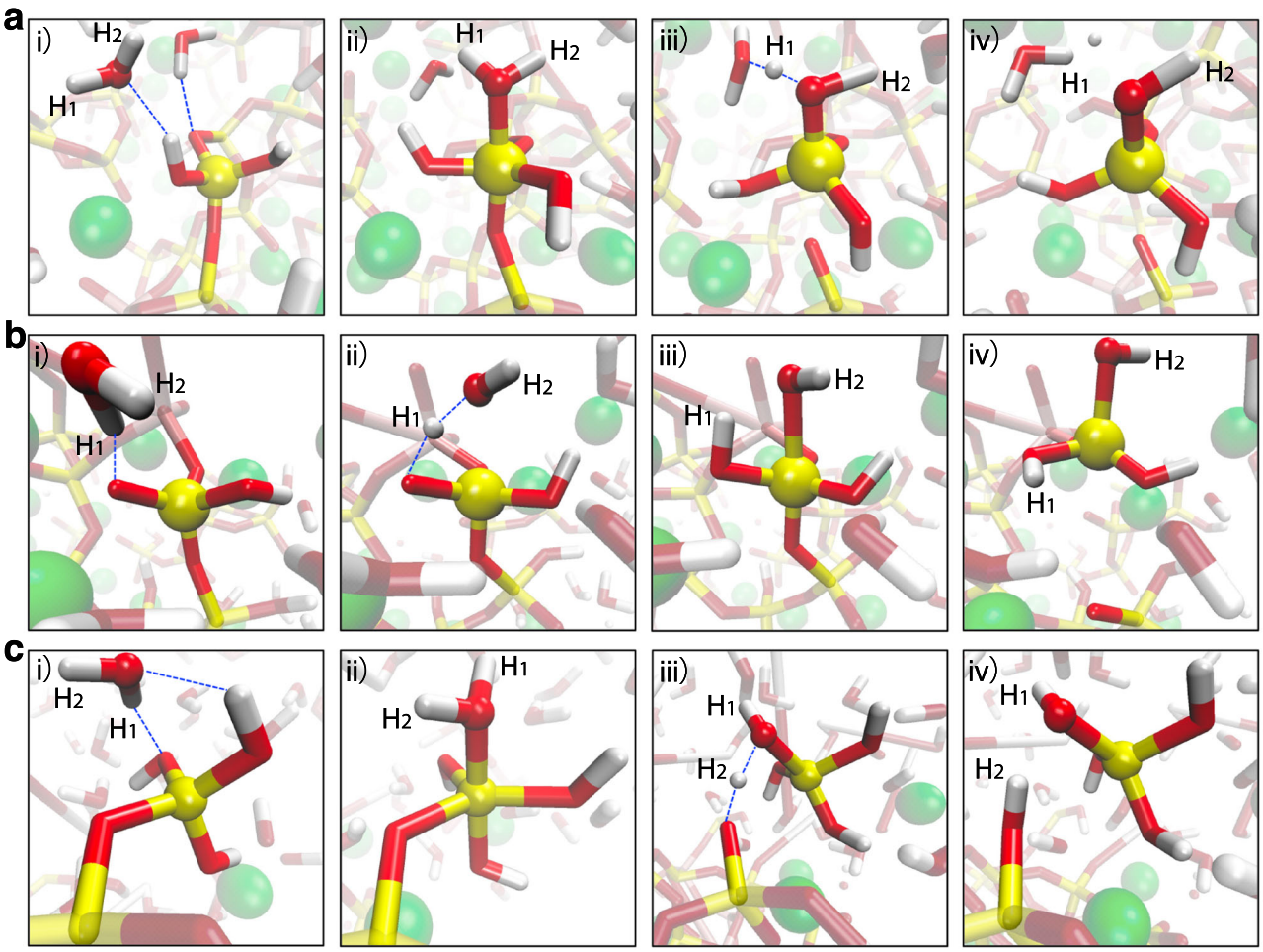

Fig. 5 | Examples depicting the destination of the proton transferred from the nucleophile under different conditions. Snapshots labeled with lowercase roman numerals indicate the sequence of events in each subplot. **a** Transfer to bulk water after coordinating to a Si Q^2. **b** Transfer to an NBO approximately at the same time as it coordinates to Si Q^2. **c** To a BO as the Si-O dissociates in Si Q^1. This behavior was observed in only one out of 60 simulations.

Contrary to the conventional wisdom, our findings point to a nucleophilic substitution reaction. This mechanism features a 5-fold coordinated Si atom with near-trigonal bipyramidal geometry, and a dissociating Si-O bond that is colinear and opposite to the coordinated nucleophile. Our study suggests that the oversimplifications in previous ab initio studies (e.g., the use of cluster systems, the absence of realistic solvent dynamics) have failed to capture this nuanced mechanism. Importantly, we have quantitatively characterized how the activation energy barrier for this reaction depends on the Si bridge coordination, identifying the dissociation of Si-O-T bridges associated to Si Q^3 species as the rate-limiting step. Our findings underscore the key roles of reorganization energy and the abundance of silanol groups in Si atoms with low bridge coordination, which serve to attract nucleophiles thereby promoting the dissociation of the remaining bridges. Through an ensemble of 60 short AIMD-WTMetaD simulations, we have unveiled variations in the reaction pathway, including the timing of proton transfer from the coordinated nucleophile water molecules and the lifetime distribution of the Si^5 intermediate or transition state, which have further enriched our mechanistic understanding of the reaction.

The findings here significantly advance our theoretical knowledge of the dissolution mechanisms and energetics of silica in calcium aluminosilicate (CAS) glasses. However, a truly comprehensive understanding of CAS glass dissolution demands further investigation into the dissociation of bridges containing alumina, as well as investigating the role of calcium on these surface reactions. Additionally, while AIMD-WTMetaD provides robust quantitative insights, the elevated computational cost underscores the need for more computationally efficient models. The development of tools like machine learning potentials or precise reactive force fields will be crucial to provide a deeper understanding of the dissolution of CAS glasses.

Computational methods

Preparation of the CAS glass–liquid water system

In this study, we modeled a CAS glass system with a stoichiometry of $(SiO_2)_{0.60}(Al_2O_3)_{0.10}(CaO)_{0.30}$, a composition previously explored for its structural, vibrational, and elastic properties[33]. We began by using molecular dynamics (MD) simulations with the reactive force field ReaxFF[34,35] to generate a bulk glass system consisting of approximately 200 atoms in a 14 Å cubic simulation box periodic in all dimensions. The detailed protocol for generating the bulk glass is described in a previous publication[22]. Next, we extended the z-dimension of the simulation box to create a slab-like glass structure. Upon breaking the periodicity of the system in the z-dimension, multiple dangling groups arising from broken T-O-T' bridges were present on the surfaces. We terminated the oxygens associated with the broken bridges with hydrogen atoms and added hydroxyl groups (-OH) to the undercoordinated Si/Al atoms at the other end of the disrupted bridges. After terminating the surfaces, we added 96 water molecules atop the glass surface and equilibrated the system to its equilibrium density, fixing all atoms within 3 Å of the bottom surface to simulate a single glass surface rather than a slab. The end result is an equilibrated, hydrated CAS glass surface. All the MD simulations were carried out using LAMMPS[36] (Large-scale Atomic/Molecular Massively Parallel Simulator package) and a time step of 0.5 fs.

Ab initio molecular dynamics–well tempered Metadynamics simulations

All the ab initio molecular dynamics (AIMD) simulations reported in this work were performed using the CP2K/Quickstep code[37,38]. These simulations were grounded in density functional theory (DFT) in the generalized gradient approximation (GGA) level of theory. Specifically, we employed the revised functional of Perdew-Burke-Ernzerhof (revPBE)[39] supplemented with Grimme's D3 dispersion corrections[40]. The electronic structure was represented using Goedecker-Teter-Hutter (GTH) pseudopotentials[41–43] for the core electrons, and a mixed Gaussian and plane waves basis (GPW) for the valence electrons[44]. For the latter, a double-ζ valence polarized (DZVP) basis set was used for Al and Ca, while a triple-zeta valence molecularly optimized basis set (TZV2P) was selected for H, O, and Si. We set a cutoff of 400 Ry for the auxiliary plane wave basis set. Periodic boundary conditions (PBC) were applied in all dimensions, and the Brillouin zone was sampled at the gamma point. The convergence criterion for the energy was set to 10^{-10} Hartree and for the self-consistent field was 10^{-6} Hartree.

All the AIMD simulations are carried out in the canonical ensemble (NVT), with a time step of 0.5 fs, and a temperature maintained at 330 K using Velocity Rescaling (CSVR) thermostat coupled to the system with a time constant of 200 fs. In our previous work we demonstrated revPBE-D3 at 330 K is the best description of liquid water at the GGA level[45,46]. All the systems are equilibrated for at least 5 ps before starting with the well-tempered Metadynamics (WTMetaD) calculations for production.

As part of the WT-MetaD[47] calculations, the bias Gaussian potential was set with a width of 0.1 (in the units of the particular collective variable) and a height of 5.25 kJ·mol^{-1}. To modulate the Gaussian heights in accordance with the well-tempered formulation, we set a fictitious temperature of 10,000 K. Regarding the collective variables (CVs) used in our study, for systems involving Q^3 and Q^2 species, the CVs represent oxygen coordination to the Si atom. This includes differentiating between bridging oxygens, denoted as CN(Si-O_b), and non-bridging or hydroxyl oxygens, CN(Si-O_W). For Q^1 systems, where only a single bridge is present, the CV related to the coordination of bridge oxygens does not provide additional insight. Consequently, in these instances, we replaced CN(Si-O_b) by Dist(Si-O_b), which measures the distance between the Si atom and the bridging oxygen. To calculate the coordination numbers, we have employed a switching function rather than a simple cutoff. Switching functions, being continuous and differentiable, facilitate smooth transitions in coordination numbers as atoms move in and out of the coordination sphere. This approach helps avoid discontinuities that could potentially affect the accuracy and reliability of the simulation results. The switching function employed is defined as follows:

$$CN(\mathrm{Si}-\mathrm{O}) = \sum_{j\in\{\mathrm{O}\}} S\left(r_{\mathrm{Si}-\mathrm{O}_j}; R_0, m, n\right) = \sum_{j\in\{\mathrm{O}\}} \frac{1-\left(\frac{r_{\mathrm{Si}-\mathrm{O}_j}}{R_0}\right)^n}{1-\left(\frac{r_{\mathrm{Si}-\mathrm{O}_j}}{R_0}\right)^m} \quad (1)$$

Where $S(r_{\mathrm{Si}-\mathrm{O}_j}; R_0, m, n)$ is a switching function bounded between 0 and 1 that describes the coordination between the Si atom under study and the oxygen atom O_j, $r_{\mathrm{Si}-\mathrm{O}_j}$ represents the distance between those atoms, R_0 serves as a decay length scale for the switching function, and m and n are tunable parameters that control the steepness of that decay. For the parameters in the switching function, we selected $n = 8$ and $m = 14$ and selected $R_0 = 2$Å based on insights from a recent study on alumina[48] and the observed differences between the Al-O and Si-O radial distribution functions (RDF) in CAS glasses[22]. To illustrate the impact of varying m and n values, we present the switching function for different parameter combinations in Supplementary Figure 3. It is worth noting that while the specific parameters of the switching function (n/m values) slightly modify the location of the free energy surface in CV space, they do not impact the fundamental findings of our study, such as the elucidated reaction mechanisms and energetics.

For the AIMD-WTMetaD simulations corresponding to the systems shown in Fig. 1, we added quadratic walls with the force constant of 100 kJ mol^{-1} to some of the CVs close to the product state to promote recrossing over the transition state and thus improve the convergence of the calculations. Specifically, for Si Q^1, we added a wall at Dist(Si-O_b) = 3.5 Å. For Si Q^2 we added a wall at CN(Si-O_W) = 3.5, and at CN(Si-O_b) = 0.5. For Q^3 CN(Si-O_b) = 0.5 and CN(Si-O_W) = 1.5.

We carried out three fully-converged AIMD-WTMetaD simulations for Si Q^1, Q^2, and Q^3 species, respectively (Fig. 1b–d), and reconstruct the free energy surface (FES) during Si-O-T bridge dissociation. In addition, to sample the diversity of variations in the Si-O-T bridge dissociation reaction, we also conducted 10 independent AIMD-WTMetaD runs for each of 6 different Si atoms on the glass surface, which were halted after the bridge dissociation event. Overall, we simulated an aggregate of over 733 ps of AIMD-WTMetaD trajectories in this study. The total production times for short simulations are shown in Supplementary Table 2.

Data availability

The data that support the findings in this study are included in the published article and its supplementary information files. Additional supporting data are available from the corresponding author upon reasonable request.

Received: 29 September 2023; Accepted: 3 March 2024;
Published online: 15 March 2024

References

1. Gin, S., Delaye, J.-M., Angeli, F. & Schuller, S. Aqueous alteration of silicate glass: state of knowledge and perspectives. *npj. Mater. Degrad.* **5**, 1–20 (2021).
2. Zanini, R., Franceschin, G., Cattaruzza, E. & Traviglia, A. A review of glass corrosion: the unique contribution of studying ancient glass to validate glass alteration models. *npj. Mater. Degrad.* **7**, 1–17 (2023).
3. Snellings, R., Suraneni, P. & Skibsted, J. Future and emerging supplementary cementitious materials. *Cem. Concr. Res.* **171**, 107199 (2023).
4. Jan, A., Delaye, J.-M., Gin, S. & Kerisit, S. Monte Carlo simulation of the corrosion of irradiated simplified nuclear waste glasses. *J. Non Cryst. Solids* **519**, 119449 (2019).
5. Ruiz Pestana, L., Shantha Raju, S., Guntoorkar, C. & Suraneni, P. Kinetic Monte Carlo study on the role of heterogeneity in the dissolution kinetics of glasses. *J. Phys. Chem. C.* **127**, 7695–7701 (2023).
6. Kurganskaya, I. & Luttge, A. Kinetic Monte Carlo simulations of silicate dissolution: model complexity and parametrization. *J. Phys. Chem. C* **117**, 24894–24906 (2013).
7. Martin, P., Gaitero, J. J., Dolado, J. S. & Manzano, H. KIMERA: a kinetic Montecarlo code for mineral dissolution. *Minerals* **10**, 825 (2020).
8. Kerisit, S. & Du, J. Monte Carlo simulation of borosilicate glass dissolution using molecular dynamics-generated glass structures. *J. Non Cryst. Solids* **522**, 119601 (2019).
9. Xiao, Y. & Lasaga, A. C. ab initio quantum mechanical studies of the kinetics and mechanisms of silicate dissolution: $H_3(H_3O^+)$ catalysis. *Geochim. Cosmochim. Acta* **58**, 5379–5400 (1994).
10. Pelmenschikov, A., Leszczynski, J. & Pettersson, L. G. M. Mechanism of dissolution of neutral silica surfaces: including effect of self-healing. *J. Phys. Chem. A* **105**, 9528–9532 (2001).
11. Icenhower, J. P. & Dove, P. M. The dissolution kinetics of amorphous silica into sodium chloride solutions: effects of temperature and ionic strength. *Geochim. Cosmochim. Acta* **64**, 4193–4203 (2000).

12. Rimstidt, J. D. & Barnes, H. L. The kinetics of silica-water reactions. *Geochim. Cosmochim. Acta* **44**, 1683–1699 (1980).
13. Criscenti, L. J., Kubicki, J. D. & Brantley, S. L. Silicate glass and mineral dissolution: calculated reaction paths and activation energies for hydrolysis of a Q^3 Si by H_3O^+ using Ab initio methods. *J. Phys. Chem. A* **110**, 198–206 (2006).
14. Masini, P. & Bernasconi, M. ab initio simulations of hydroxylation and dehydroxylation reactions at surfaces: amorphous silica and brucite. *J. Phys.: Condens. Matter* **14**, 4133 (2002).
15. Rimola, A. & Ugliengo, P. A quantum mechanical study of the reactivity of $(SiO)_2$-defective silica surfaces. *J. Chem. Phys.* **128**, 204702 (2008).
16. Bouyer, F., Geneste, G., Ispas, S., Kob, W. & Ganster, P. Water solubility in calcium aluminosilicate glasses investigated by first principles techniques. *J. Solid. State Chem.* **183**, 2786–2796 (2010).
17. Rimsza, J. M. & Du, J. Ab initio molecular dynamics simulations of the hydroxylation of nanoporous silica. *J. Am. Ceram. Soc.* **98**, 3748–3757 (2015).
18. Rimsza, J. M., Yeon, J., van Duin, A. C. T. & Du, J. Water interactions with nanoporous silica: comparison of ReaxFF and ab initio based molecular dynamics simulations. *J. Phys. Chem. C* **120**, 24803–24816 (2016).
19. Michalske, T. A. & Freiman, S. W. A molecular mechanism for stress corrosion in vitreous silica. *J. Am. Ceram. Soc.* **66**, 284–288 (1983).
20. Carter, E. A., Ciccotti, G., Hynes, J. T. & Kapral, R. Constrained reaction coordinate dynamics for the simulation of rare events. *Chem. Phys. Lett.* **156**, 472–477 (1989).
21. Ceresoli, D., Bernasconi, M., Iarlori, S., Parrinello, M. & Tosatti, E. Two-membered silicon rings on the dehydroxylated surface of silica. *Phys. Rev. Lett.* **84**, 3887–3890 (2000).
22. Liu, M., Panda, S., Suraneni, P. & Ruiz Pestana, L. Insights from molecular dynamics into the chemistry-structure relationships of calcium aluminosilicate glasses. *J. Non Cryst. Solids* **618**, 122545 (2023).
23. Wallace, A. F., Gibbs, G. V. & Dove, P. M. Influence of ion-associated water on the hydrolysis of Si−O bonded interactions. *J. Phys. Chem. A* **114**, 2534–2542 (2010).
24. Morrow, C. P., Nangia, S. & Garrison, B. J. Ab initio investigation of dissolution mechanisms in aluminosilicate minerals. *J. Phys. Chem. A* **113**, 1343–1352 (2009).
25. Izadifar, M., Ukrainczyk, N. & Koenders, E. Silicate dissolution mechanism from metakaolinite using density functional theory. *Nanomaterials (Basel)* **13**, 1196 (2023).
26. Kagan, M., Lockwood, G. K. & Garofalini, S. H. Reactive simulations of the activation barrier to dissolution of amorphous silica in water. *Phys. Chem. Chem. Phys.* **16**, 9294–9301 (2014).
27. Yeon, J. & van Duin, A. C. T. ReaxFF molecular dynamics simulations of hydroxylation kinetics for amorphous and nano-silica structure, and its relations with atomic strain energy. *J. Phys. Chem. C* **120**, 305–317 (2016).
28. Kalahe, J. et al. Composition effect on interfacial reactions of sodium aluminosilicate glasses in aqueous solution. *J. Phys. Chem. B* **127**, 269–284 (2023).
29. Kalahe, J. et al. Temperature dependence of interfacial reactions of sodium aluminosilicate glasses from reactive molecular dynamics simulations. *Appl. Surf. Sci.* **619**, 156780 (2023).
30. E, W., Ren, W. & Vanden-Eijnden, E. Finite temperature string method for the study of rare events. *J. Phys. Chem. B* **109**, 6688–6693 (2005).
31. Pestana, L. R., Hao, H. & Head-Gordon, T. Diels–Alder reactions in water are determined by microsolvation. *Nano. Lett.* **20**, 606–611 (2020).
32. Nesbitt, H. W., Bancroft, G. M. & Henderson, G. S. Nucleophilic substitution reaction mechanisms: An atomic-molecular perspective on chemical speciation and transport properties in silicate melts. *Chem. Geol.* **555**, 119818 (2020).
33. Bauchy, M. Structural, vibrational, and elastic properties of a calcium aluminosilicate glass from molecular dynamics simulations: The role of the potential. *J. Chem. Phys.* **141**, 024507 (2014).
34. Leven, I. et al. Recent Advances for Improving the Accuracy, Transferability, and Efficiency of Reactive Force Fields. *J. Chem. Theory Comput.* **17**, 3237–3251 (2021).
35. Senftle, T. P. et al. The ReaxFF reactive force-field: development, applications and future directions. *npj Comput. Mater.* **2**, 1–14 (2016).
36. Plimpton, S. Fast parallel algorithms for short-range molecular dynamics. *J. Comput. Phys.* **117**, 1–19 (1995).
37. Hutter, J., Iannuzzi, M., Schiffmann, F. & VandeVondele, J. cp2k: atomistic simulations of condensed matter systems. *WIREs Comput. Mol. Sci.* **4**, 15–25 (2014).
38. VandeVondele, J. et al. Quickstep: fast and accurate density functional calculations using a mixed Gaussian and plane waves approach. *Comput. Phys. Commun.* **167**, 103–128 (2005).
39. Perdew, J. P., Burke, K. & Ernzerhof, M. Generalized gradient approximation made simple. *Phys. Rev. Lett.* **77**, 3865–3868 (1996).
40. Grimme, S., Antony, J., Ehrlich, S. & Krieg, H. A consistent and accurate ab initio parametrization of density functional dispersion correction (DFT-D) for the 94 elements H-Pu. *J. Chem. Phys.* **132**, 154104 (2010).
41. Krack, M. Pseudopotentials for H to Kr optimized for gradient-corrected exchange-correlation functionals. *Theor. Chem. Acc.* **114**, 145–152 (2005).
42. Goedecker, S., Teter, M. & Hutter, J. Separable dual-space Gaussian pseudopotentials. *Phys. Rev. B* **54**, 1703–1710 (1996).
43. Hartwigsen, C., Goedecker, S. & Hutter, J. Relativistic separable dual-space Gaussian pseudopotentials from H to Rn. *Phys. Rev. B* **58**, 3641–3662 (1998).
44. VandeVondele, J. & Hutter, J. Gaussian basis sets for accurate calculations on molecular systems in gas and condensed phases. *J. Chem. Phys.* **127**, 114105 (2007).
45. Ruiz Pestana, L., Mardirossian, N., Head-Gordon, M. & Head-Gordon, T. ab initio molecular dynamics simulations of liquid water using high quality meta-GGA functionals. *Chem. Sci.* **8**, 3554–3565 (2017).
46. Ruiz Pestana, L., Marsalek, O., Markland, T. E. & Head-Gordon, T. The Quest for Accurate Liquid Water Properties from First Principles. *J. Phys. Chem. Lett.* **9**, 5009–5016 (2018).
47. Barducci, A., Bussi, G. & Parrinello, M. Well-tempered metadynamics: a smoothly converging and tunable free-energy method. *Phys. Rev. Lett.* **100**, 020603 (2008).
48. Réocreux, R. et al. Reactivity of shape-controlled crystals and metadynamics simulations locate the weak spots of alumina in water. *Nat. Commun.* **10**, 3139 (2019).

Acknowledgements

We would like to thank the National Science Foundation for funding support under Grant No. 2101961. L.R.P. is also thankful for the endowment support from Dr. Reza and Georgianna Khatib. We are grateful to Dr. Prannoy Suraneni for fruitful discussions. All the simulations shown in this study were carried out using the supercomputer Triton, managed by the Institute of Data Science and Computing (IDSC) at the University of Miami.

Author contributions

M.L. executed the simulations and led the data analysis. L.R.P. contributed to conceptualization, supervision, and manuscript writing. Both authors discussed the results, collaborated on the development of the original draft, and contributed to reviewing and editing subsequent versions.

Competing interests

The authors declare no competing interests.

Additional information

Supplementary information The online version contains supplementary material available at https://doi.org/10.1038/s41529-024-00445-x.

Correspondence and requests for materials should be addressed to Luis Ruiz Pestana.